 Copy 44
RM SL55D15

NACA

RESEARCH MEMORANDUM

for the

Bureau of Aeronautics, Department of the Navy

LOW-LIFT DRAG OF THE GRUMMAN F9F-9 AIRPLANE AS OBTAINED BY A 1/7.5-SCALE ROCKET-BOOSTED MODEL AND BY THREE 1/45.85-SCALE EQUIVALENT-BODY MODELS BETWEEN MACH NUMBERS OF 0.8 AND 1.3

TED No. NACA DE ~~390~~ 391

By Joseph E. Stevens

Langley Aeronautical Laboratory
Langley Field, Va.

NATIONAL ADVISORY COMMITTEE FOR AERONAUTICS

WASHINGTON

NACA RM SL55D15

NATIONAL ADVISORY COMMITTEE FOR AERONAUTICS

RESEARCH MEMORANDUM

for the

Bureau of Aeronautics, Department of the Navy

LOW-LIFT DRAG OF THE GRUMMAN F9F-9 AIRPLANE AS OBTAINED BY A 1/7.5-SCALE ROCKET-BOOSTED MODEL AND BY THREE 1/45.85-SCALE EQUIVALENT-BODY MODELS BETWEEN MACH NUMBERS OF 0.8 AND 1.3

TED No. NACA DE ~~390~~ 391

By Joseph E. Stevens

SUMMARY

Low-lift drag data are presented herein for one 1/7.5-scale rocket-boosted model and three 1/45.85-scale equivalent-body models of the Grumman F9F-9 airplane. The data were obtained over a Reynolds number range of about 5×10^6 to 10×10^6 based on wing mean aerodynamic chord for the rocket model and total body length for the equivalent-body models.

The rocket-boosted model showed a drag rise of about 0.037 (based on included wing area) between the subsonic level and the peak supersonic drag coefficient at the maximum Mach number of this test. The base drag coefficient measured on this model varied from a value of -0.0015 in the subsonic range to a maximum of about 0.0020 at a Mach number of 1.28.

Drag coefficients for the equivalent-body models varied from about 0.125 (based on body maximum area) in the subsonic range to about 0.300 at a Mach number of 1.25. Increasing the total fineness ratio by a small amount raised the drag-rise Mach number slightly.

INTRODUCTION

The Langley Pilotless Aircraft Research Division, at the request of the Bureau of Aeronautics, Department of the Navy, has conducted low-lift

drag tests of six models of the Grumman F9F-9 airplane. Three 1/7.5-scale rocket-boosted conventional models were tested in free flight and three 1/45.85-scale equivalent-body-area models were flown from the 6-inch helium gun. No data were obtained from the first two rocket-boosted models because the first failed to separate from its booster and the second maneuvered so violently during the early portion of the test that radar tracking was impossible. Data were obtained from the third rocket-boosted model and from all the equivalent-body models.

The rocket-boosted model duplicated the prototype airplane as it was built, whereas the equivalent-body models represented the F9F-9 configuration at two earlier points in the airplane development.

The Grumman F9F-9 is a jet-propelled, swept-wing, interceptor-type airplane designed for transonic speeds. Twin side scoops with boundary-layer bleeds are placed ahead of the wing, and the fuselage area is diminished in the region of the wing in order to provide a reasonable area distribution. Conventional tail surfaces are incorporated in the design with the all-movable horizontal tail being placed just below the extended wing-chord plane.

The purpose of the tests reported herein was to determine the low-lift drag of the complete airplane configuration at transonic and low supersonic speeds.

SYMBOLS

A	cross-sectional area, sq in.
a_l/g	acceleration along longitudinal axis as obtained from accelerometer, g units (positive forward)
c	wing chord, ft
$\bar{c}$	wing mean aerodynamic chord, 1.117 ft
C_D	drag coefficient
g	acceleration due to gravity, value taken as 32.2 ft/sec^2
l	basic model body length, in.
M	Mach number
$\frac{\Delta P_a}{q}$	rocket-model exit-annulus base pressure coefficient

$\frac{\Delta P_c}{q}$	rocket-model choking-cup base pressure coefficient
q	dynamic pressure, lb/sq ft
R	Reynolds number
r	helium-gun-model body radius, in.
S_a	rocket-model base-annulus area, 0.0307 sq ft
S_B	helium-gun-model maximum cross-sectional area, 0.0123 sq ft
S_C	rocket-model choking-cup base area, 0.0244 sq ft
S_W	rocket-model included wing area, 4.54 sq ft
t	time, sec
V	velocity, ft/sec
W	model weight, lb
x	model station measured back from nose, in.
γ	flight-path angle, deg

MODELS AND INSTRUMENTATION

Rocket Models

Figure 1 is a three-view sketch of the identical second and third 1/7.5-scale rocket-boosted models used in this investigation. The first model flown was different in several respects (no boundary-layer bleed, smaller horizontal tail, slightly shorter nose, and others) but no drawing is presented since no data could be obtained from the test flight because of the failure of the model to separate from its booster assembly. However, wind-tunnel data for a model similar to model 1 can be found in references 1 and 2. Data from reference 1 were used in the selection of the tail incidence angle for the rocket-boosted models to provide near-zero lift throughout the test Mach number range. The geometric characteristics of model 3 are given in table I and photographs of the model and the model-booster combination mounted on the zero-length launcher are shown in figure 2.

All the models had internal air flow and a choking cup in the duct exit to provide a mass-flow ratio of approximately 0.8 at M = 1.0. Figure 3 presents the area distribution of model 3 with a breakdown of some of the component parts. The area of the fuselage in the region of the duct has been reduced by an area equal to 80 percent of the inlet area to make allowance for the air flow through the model.

The rocket models were constructed largely of wood reinforced with metal. The fuselage was built of mahogany fabricated around a $3\frac{1}{2}$-inch-diameter steel tube which extended from about the leading edge of the wing-fuselage intersection station to the base of the fuselage. Longitudinal steel webs and a bulkhead extended forward from the tube to support the fiber-glass-reinforced plastic nose, the mahogany fuselage blocks, and the duct inlets, whereas the wing, the rear fuselage blocks, and the tail surfaces were bolted directly to the tube. The tube itself also served as the rear portion of the internal ducting and absorbed the thrust of the booster rocket used to accelerate the model to supersonic speeds. The model wings were constructed of wood laminated on an aluminum-alloy core plate and the tail surfaces were machined from solid aluminum alloy. The entire model was covered with a thin layer (0.005 in.) of fiber-glass-reinforced plastic.

The nose of the third model contained a standard NACA four-channel telemeter transmitter. A probe extending forward from the nose of the model and connected to an internal pressure-measuring pickup was used to determine total pressure, an accelerometer located near the center of gravity measured accelerations along the longitudinal body axis, and two pressure-measuring pickups located near the tail were used to ascertain base pressure on the exit annulus and at the base of the throttling cup placed in the duct exit to control the mass-flow ratio through the duct. Figure 4 is a photograph of the duct exit showing four pressure orifices on the annulus and the orifice at the base of the throttling cup. The annulus orifices were manifolded and one pressure measurement taken to obtain base-annulus-pressure data.

The cracks, joints, and bolt holes that appear in all the photographs of the model were filled and faired smooth before the test flight.

In addition to the model telemetering instrumentation, a CW Doppler radar set was used to obtain the velocity of the model during the test flight and a modified SCR 584 tracking radar set provided space-location data. A radiosonde released immediately after the model flight supplied atmospheric data for the test.

Helium-Gun Models

A sketch of the 1/45.85-scale helium-gun models is shown in figure 5 and the model ordinates are given in table II. Models A and B, which were identical, are shown in figure 5(a) and model C, which had a longer nose section, is shown in figure 5(b). A photograph of models A and B is shown as figure 6. The models were bodies of revolution with area distributions equivalent to the total airplane configuration as it was planned when the models were designed. The model area in the vicinity of the stabilizing fins was reduced by the actual cross-sectional area of the stabilizing fins in order to make the area distribution of the total model configuration equivalent to the airplane. Figure 7 presents the area distributions of the models as a function of the basic model length from the nose to the duct exit station with 80 percent of the inlet area removed. A comparison of figure 7 and figure 3 readily shows some of the changes which the F9F-9 configuration underwent during the portion of its development which the models used in this investigation represent. As mentioned in the "Introduction" section, the equivalent-body models represented two configurations developed during the design of the airplane, whereas the rocket model simulated the prototype airplane as it was built.

The helium-gun models were constructed entirely of aluminum alloy and were stabilized in flight by three aluminum fins attached to the rear part of the models. The models were accelerated from the 6-inch-diameter barrel with approximately 200 lb/sq in. helium pressure at an elevation angle of about 20°. An aluminum cup filled with a hard plastic material contoured to fit the model rear end transmitted the gas-pressure thrust from a metal-reinforced plywood push plate to the model. A three-piece balsa sabot alined the models in the barrel (see ref. 3). The cup, push plate, and sabot were designed to separate from the model immediately upon exit from the barrel muzzle. A CW Doppler radar set was alined with the flight path of the model and measured the velocity of the model during the major portion of the coasting flight. Atmospheric data were obtained immediately after the test from ground observations and low-altitude radiosonde.

METHODS OF ANALYSIS

The rocket-model drag data presented herein were obtained during the coasting portion of the test flight after the model had separated from its booster. Total drag coefficients C_{D_T} were obtained from the relationship

$$C_{D_T} = -\frac{a_z}{g}\frac{W}{qS_W}$$

Dynamic pressure was determined from the relationship of total pressure to static pressure. The static pressure was obtained by using radiosonde data in conjunction with flight-path data obtained by radar.

The external-drag coefficients $C_{D_{ext}}$ were determined from the equation

$$C_{D_{ext}} = C_{D_T} - C_{D_{base}} - C_{D_{int}}$$

where base drag coefficients $C_{D_{base}}$ were determined from the telemetered base-pressure data as follows:

$$-C_{D_{base}} = \frac{\Delta P_a}{q}\frac{S_a}{S_W} + \frac{\Delta P_c}{q}\frac{S_c}{S_W}$$

Internal-drag coefficients $C_{D_{int}}$ were obtained from reference 4, which presents data from a preflight duct calibration test of the rocket-model configuration. Although it is possible for the internal-drag coefficient from this test to be somewhat in error (±10 percent or more), the magnitude of $C_{D_{int}}$ is so small in comparison to $C_{D_{ext}}$ that the overall percentage error is quite small.

Drag-coefficient data for the helium-gun models were calculated by using the equation

$$C_D = -\left(\frac{dV}{dt} + g \sin \gamma\right)\frac{W}{gqS_B}$$

where dyanmic pressure q was determined by using density obtained by radiosonde and velocity corrected for wind; the flight-path angle γ and the altitude were determined from calculated zero-lift trajectories.

DISCUSSION OF RESULTS

Figure 8 presents scale data for the tests reported herein. The Reynolds number of the rocket-model test based on wing mean aerodynamic chord (fig. 8(a)) varied from about 5×10^6 at $M = 0.82$ to 9×10^6 at $M = 1.28$. Figure 8(b) shows that the Reynolds number (based on total

body length) of the helium-gun-model tests varied from about 5×10^6 at $M = 0.80$ to about 10×10^6 at $M = 1.30$.

Figure 9 presents a summary of the drag data (based on included wing area) measured for the 1/7.5-scale rocket-boosted model. The total-drag-coefficient curve shows a subsonic drag level of about 0.016 with the drag rise $\left(\text{at } \frac{dC_D}{dM} = 0.1 \text{ for winged models}\right)$ occurring at a Mach number of about 0.94 and a peak pressure drag of approximately 0.037 with the maximum C_D at $M \approx 1.28$, which is the upper limit of this test. The "drag bucket" which occurs at $M \approx 0.98$ is thought to be function of the movement of an expansion wave on the boattailed portion of the rear fuselage. A similar drag variation is included in the data for other configurations in references 5 and 6.

Base-drag-coefficient data also shown in figure 9 indicate a subsonic value of about -0.0015, increasing through zero at $M = 1.00$ and to about 0.0020 at $M = 1.28$. A "bucket" also appears in the region between $M = 0.98$ and $M = 1.00$; this result supports the idea that the cause is probably due to air-flow effects over the rear portion of the fuselage. The phenomenon appeared in the measurements of base pressure both on the base annulus and the choking cup but to a smaller degree on the cup. In analyzing the base-drag data, it was found that the annulus base drag amounted to about twice the amount attributable to the throttling-cup base drag.

The internal-drag-coefficient curve obtained from reference 4 is presented in figure 9 and remains relatively constant throughout the Mach number range tested.

External-drag-coefficient data (fig. 9) varies from about 5 percent below the total-drag data at $M = 1.28$ to about 4 percent above in the subsonic region with a mass-flow ratio of about 0.80 at $M = 1.0$.

Drag data for the three 1/45.85-scale equivalent-body models are shown in figure 10. Models A and B, which were identical, indicate the degree of repeatability that can be expected from tests using the helium-gun technique. Models A and B show a subsonic C_D of about 0.125 (based on maximum body cross-sectional area) and a peak pressure-drag coefficient of about 0.175 with the peak C_D of 0.300 occurring at approximately $M = 1.25$. The drag rise of these two models begins at $M = 0.97$ $\left(\frac{dC_D}{dM} = 1.0 \text{ for wingless models}\right)$. Model C, with a higher total fineness ratio, exhibits about the same subsonic drag level but a slightly higher

peak drag ($C_D = 0.325$ at $M = 1.30$) and the drag rise occurs at a slightly higher Mach number ($M = 0.99$). The increase in drag-rise Mach number is as would be expected, but the higher supersonic drag is opposite to what would be expected for an increase in fineness ratio.

At the time the equivalent-body models were conceived and designed (early 1953) it was thought that a good approximation of the configuration peak pressure drag could be obtained. Since that time, tests have shown that very poor correlation is obtained by using the equivalent-body method for swept-wing configurations (ref. 7). For this reason and the changes that exist in the configuration between the equivalent-body models and the rocket model, no attempt has been made to compare the peak pressure drags.

SUMMARY OF RESULTS

An investigation of the low-lift drag of a 1/7.5-scale rocket-boosted model and three 1/45.85-scale equivalent-body models of the Grumman F9F-9 configuration provided the following results:

1. The total drag coefficient for the 1/7.5-scale rocket-boosted model indicated a drag rise of about 0.037 (based on included wing area) with a drag-rise Mach number of about 0.94.

2. The base drag coefficient for the 1/7.5-scale model varied from a level of about -0.0015 in the subsonic range to a maximum of about 0.0020 at a Mach number of 1.28.

3. Drag coefficients for the original equivalent-body models varied from 0.125 (based on body maximum area) at subsonic speeds to 0.300 at a Mach number of 1.25.

Langley Aeronautical Laboratory,
National Advisory Committee for Aeronautics,
Langley Field, Va., March 24, 1955.

Joseph E. Stevens
Aeronautical Research Scientist

Approved:
Joseph A. Shortal
Chief of Pilotless Aircraft Research Division

rmw

REFERENCES

1. Bielat, Ralph P.: A Transonic Wind-Tunnel Investigation of the Performance and of the Static Stability and Control Characteristics of a 1/15-Scale Model of the Grumman F9F-9 Airplane - TED No. NACA DE 390. NACA RM SL54J15, Bur. Aero., 1954.

2. Palazzo, Edward B., and Spearman, M. Leroy: Static Longitudinal and Lateral Stability and Control Characteristics of a 1/5-Scale Model of the Grumman F9F-9 Airplane at a Mach Number of 1.41 - TED No. NACA DE 390. NACA RM SL54G08, Bur. Aero., 1954.

3. Stevens, Joseph E., and Purser, Paul E.: Flight Measurements of the Transonic Drag of Models of Several Isolated External Stores and Nacelles. NACA RM L54I07, 1954.

4. Roukis, J. G.: Test Result of F9F-9 Rocket-Fired Model #1 Direct Connect Duct Calibration Tests at Wright Aero. Rep. No. XA98-A2-6.2 (Contract No. NOa(s)-53-1013), Grumman Aircraft Eng. Corp., Dec. 29, 1953. (Revised 1954, Rep. No. XA98-C-6.2.)

5. Purser, Paul E.: Comparison of Wind-Tunnel, Rocket, and Flight Drag Measurements for Eight Airplane Configurations at Mach Numbers Between 0.7 and 1.6. NACA RM L54F18, 1954.

6. Wallskog, Harvey A.: Summary of Free-Flight Zero-Lift Drag Results From Tests of 1/5-Scale Models of the Convair YF-102 and F-102A Airplanes and Several Related Small Equivalent Bodies at Mach Numbers From 0.70 to 1.46. NACA RM SL54J25, U. S. Air Force, 1954.

7. Whitcomb, Richard T.: Recent Results Pertaining to the Application of the "Area Rule." NACA RM L53I15a, 1953.

TABLE I

ROCKET-MODEL GEOMETRIC CHARACTERISTICS

Wing:	
Airfoil section at root (free-stream)	NACA 65A006(mod.)
Airfoil section at tip (free-stream)	NACA 65A004(mod.)
Area (included), sq ft	1.54
Aspect ratio	3.92
Taper ratio	0.49
Sweepback (quarter chord), deg	35
Incidence, deg	0
Dihedral, deg	-2.50
Horizontal tail:	
Airfoil section at root (free-stream)	NACA 65A006
Airfoil section at tip (free-stream)	NACA 65A004
Area (included), sq ft	1.22
Aspect ratio	3.65
Taper ratio	0.40
Sweepback (quarter chord), deg	35
Incidence, deg	-0.63
Dihedral, deg	0
Vertical tail (see fig. 4):	
Airfoil section (free-stream)	NACA 0006
Area, sq ft	0.71
Aspect ratio	3.02
Taper ratio	0.18
Duct and base areas:	
Duct inlet, sq in.	8.16
Duct exit, sq in.	6.82
Base annulus, sq in.	4.42
Cup base, sq in.	3.51

TABLE II

ORDINATES OF 1/45.85-SCALE MODELS

Models A and B		Model C	
x, in.	r, in.	x, in.	r, in.
0	0	0	0
.500	.228	.090	.050
1.000	.350	.590	.220
1.500	.458	1.090	.300
2.000	.525	1.590	.370
2.500	.570	2.090	.450
2.573	.574	2.590	.510
2.573	.603	3.090	.560
3.000	.663	3.445	.574
3.500	.700	3.445	.603
4.000	.725	3.590	.620
4.500	.740	4.090	.670
5.000	.748	4.663	.705
5.393	.750	5.090	.725
5.500	.749	5.590	.740
6.000	.743	6.090	.748
6.500	.725	6.483	.750
7.000	.695	6.590	.749
7.500	.650	7.090	.743
8.000	.598	7.590	.725
8.500	.540	8.090	.695
9.000	.474	8.590	.650
9.500	.408	9.090	.598
9.703	.362	9.590	.540
9.703	.335	10.090	.474
10.673	.185	10.590	.408
11.643	.035	10.793	.362
		11.763	.185
		12.733	.035
Basic length l, 9.703 in.		Basic length l, 10.793 in.	

CONFIDENTIAL

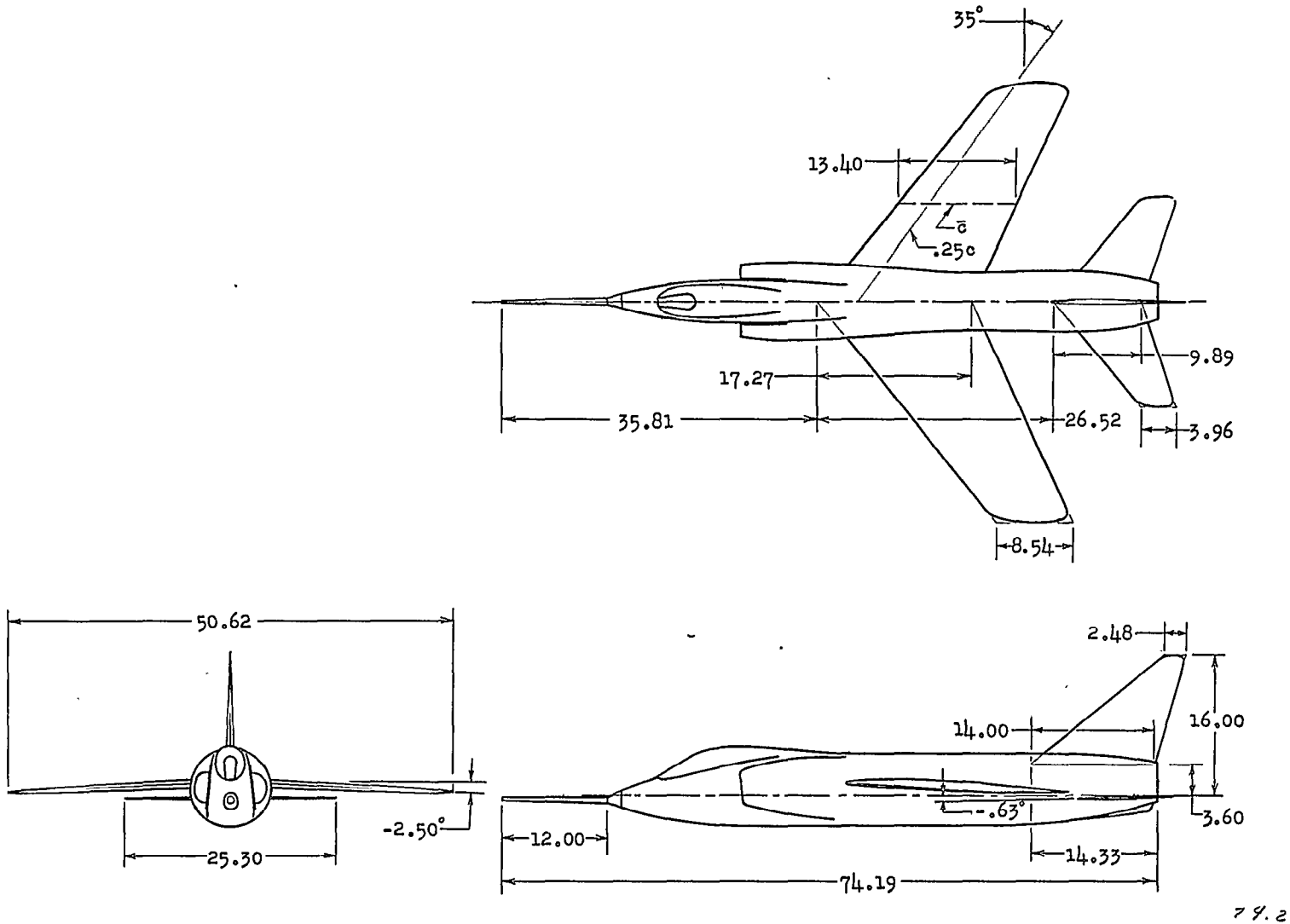

Figure 1.- Three-view sketch of rocket-boosted model 3. All dimensions are in inches unless noted.

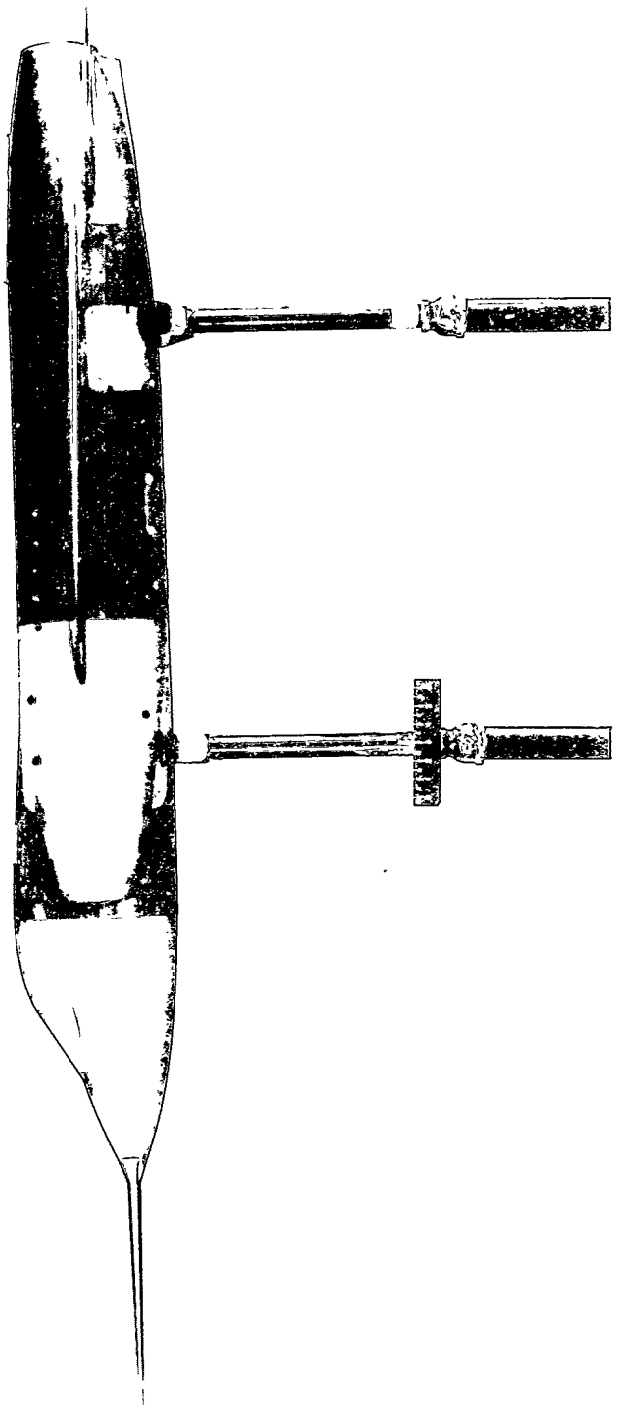

L-85967.1

(a) Side view.

Figure 2.- Photographs of rocket model 3.

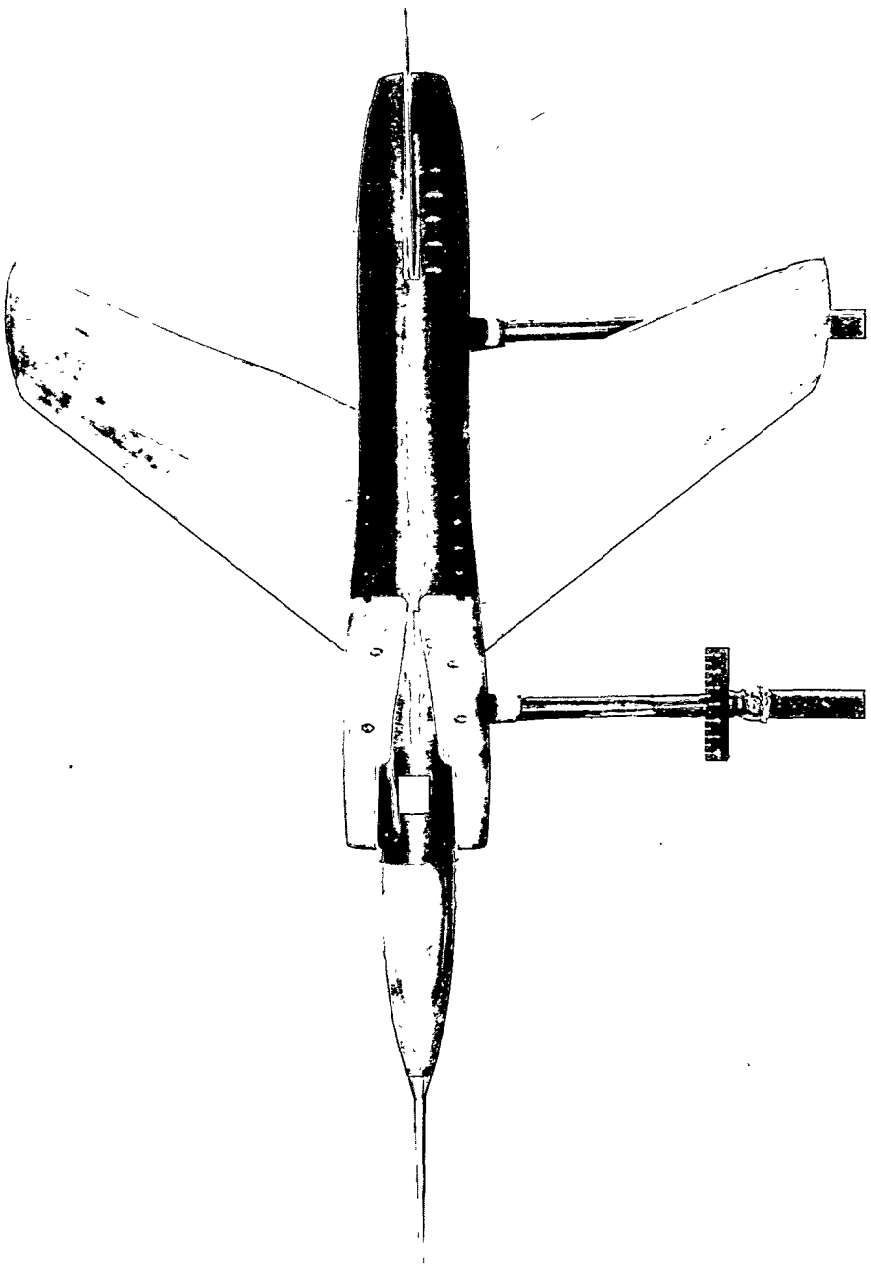

L-85966.1

(b) Top view.

Figure 2.- Continued.

L-85965.1

(c) Three-quarter front view.

Figure 2.- Continued.

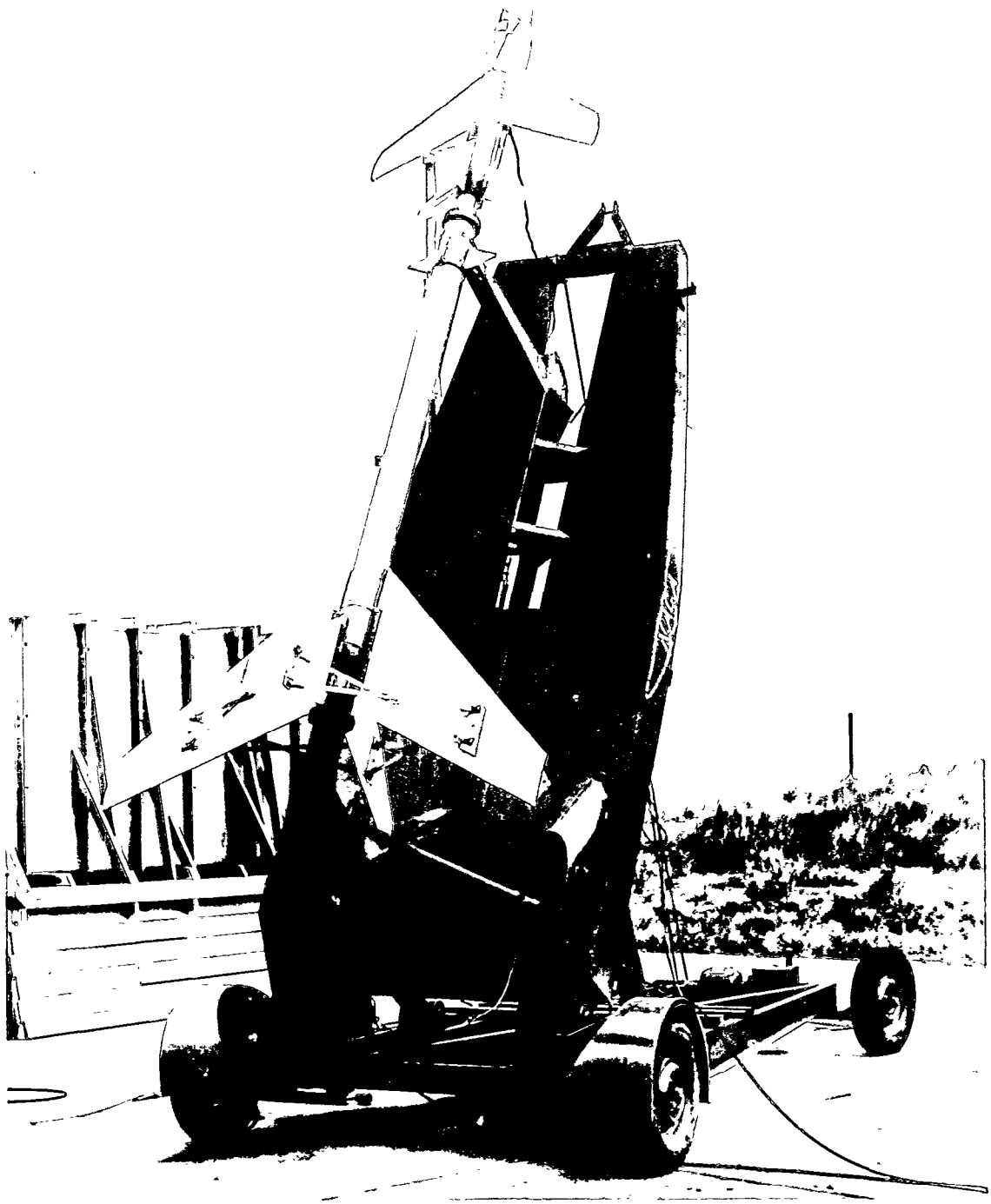

L-86328.1

(d) Model 3 and booster mounted on launcher.

Figure 2.- Concluded.

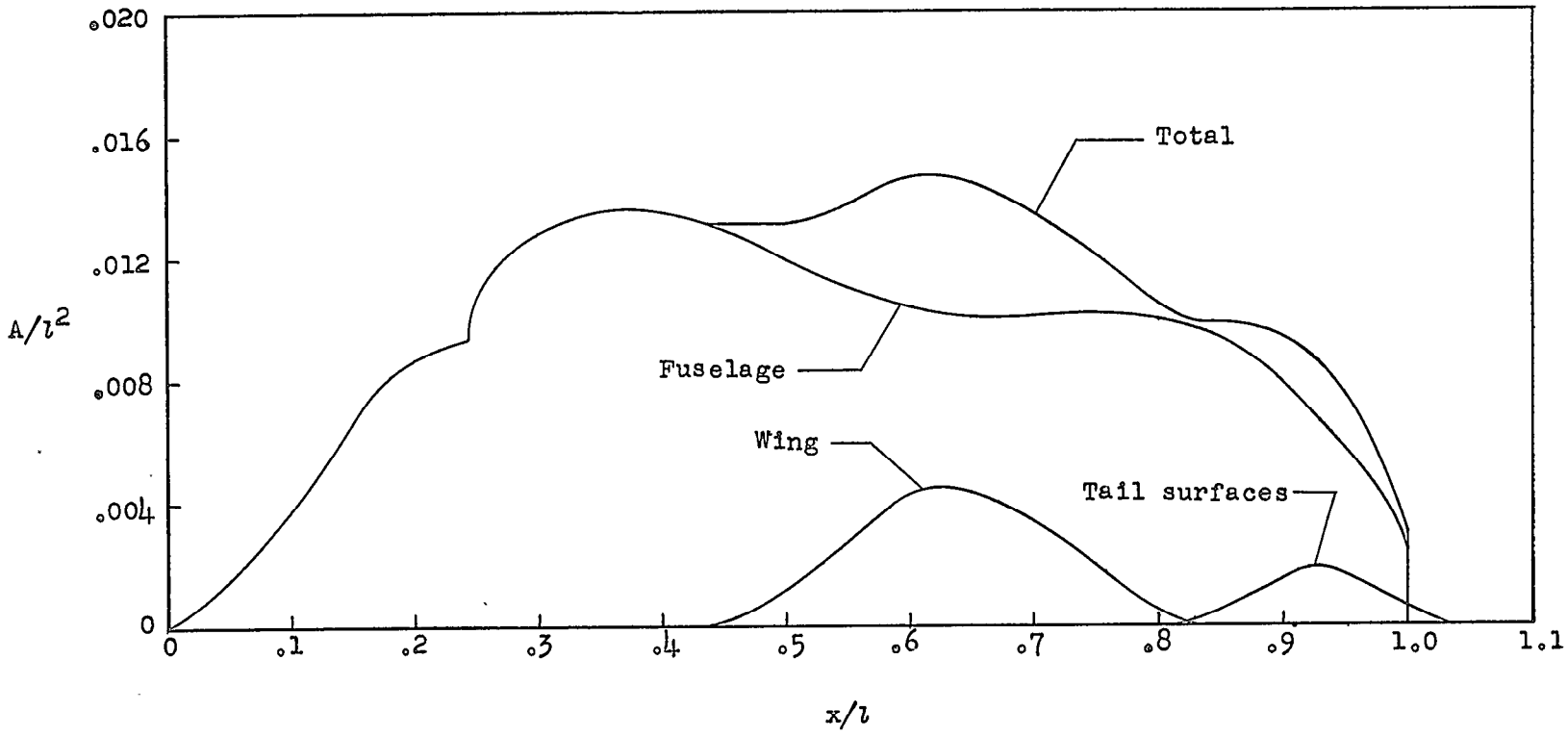

Figure 3.- Longitudinal area distribution of rocket model 3 as a function of basic body length (l = 62.267 inches).

L-85964.1

Figure 4.- Photograph of the fuselage base of rocket model 3 showing the base pressure-measuring orifices.

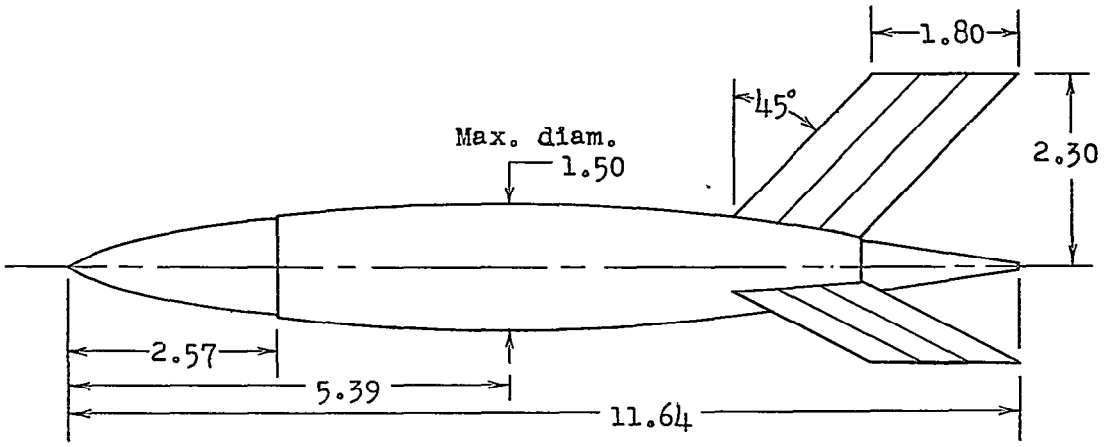

(a) Models A and B (total fineness ratio, 7.762).

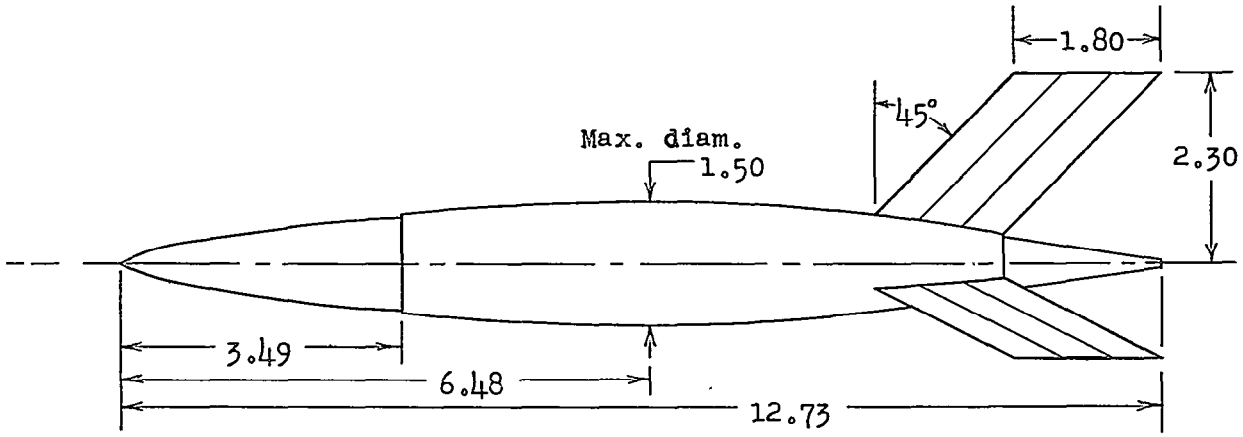

(b) Model C (total fineness ratio, 8.489).

Figure 5.- Sketches of the 1/45.85-scale equivalent-body models. All dimensions are in inches unless noted.

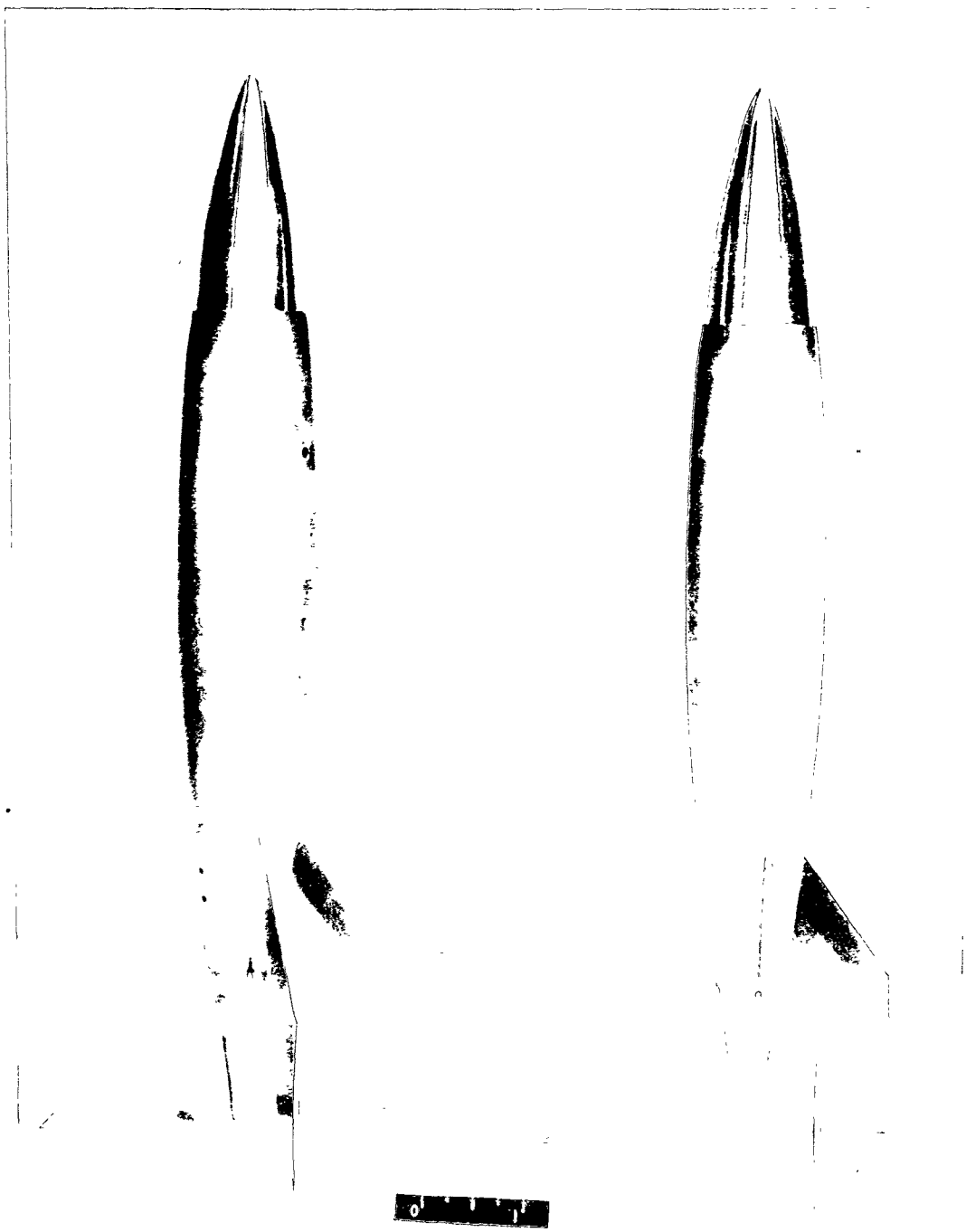

Figure 6.- Photograph of models A and B. L-79909

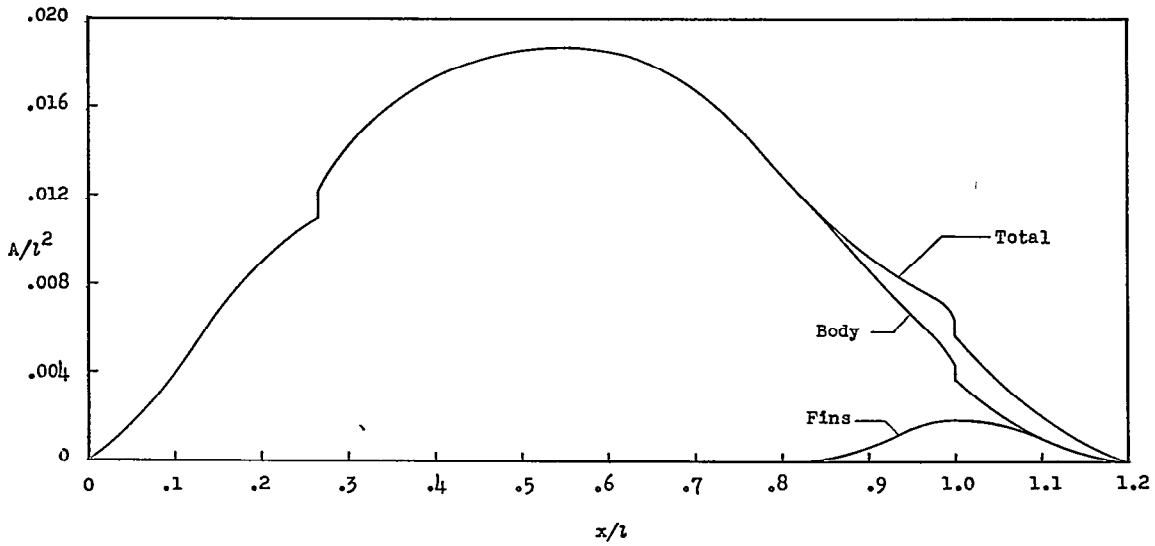

(a) Models A and B (l = 9.703 inches).

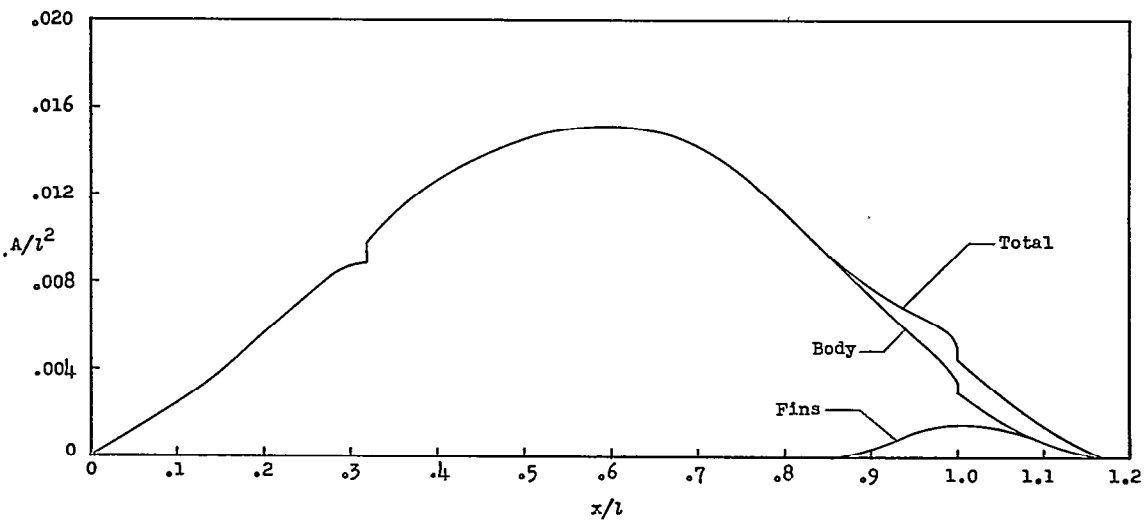

(b) Model C (l = 10.793 inches).

Figure 7.- Longitudinal area distribution as a function of basic body length.

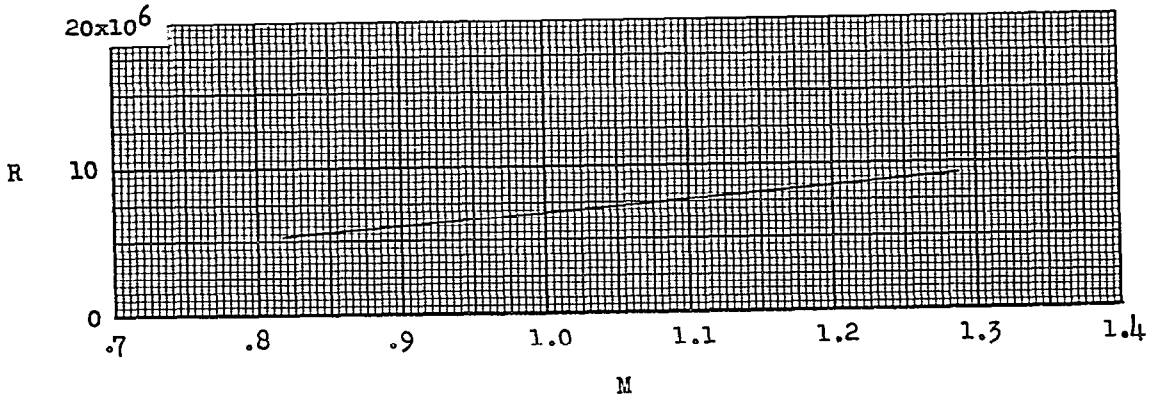

(a) Rocket model 3 (based on wing M.A.C.).

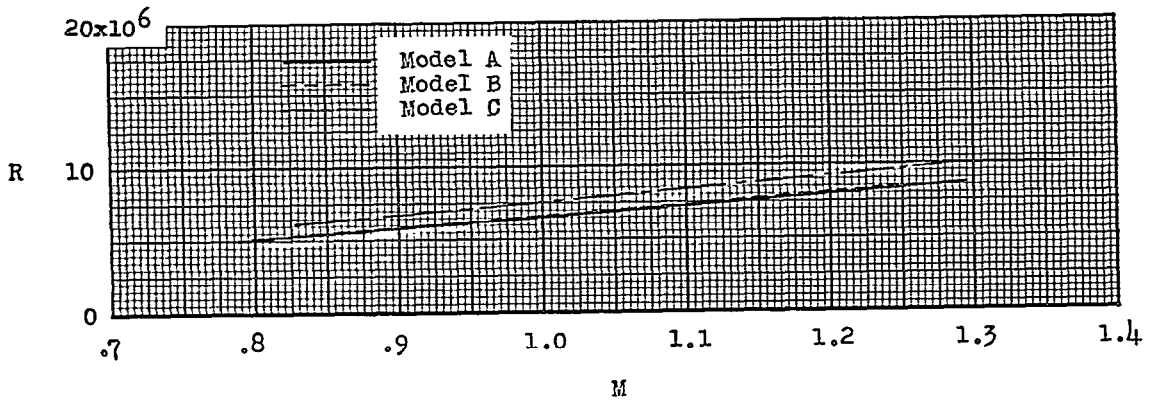

(b) Models A, B, and C (based on body length).

Figure 8.- Reynolds number as a function of test Mach number.

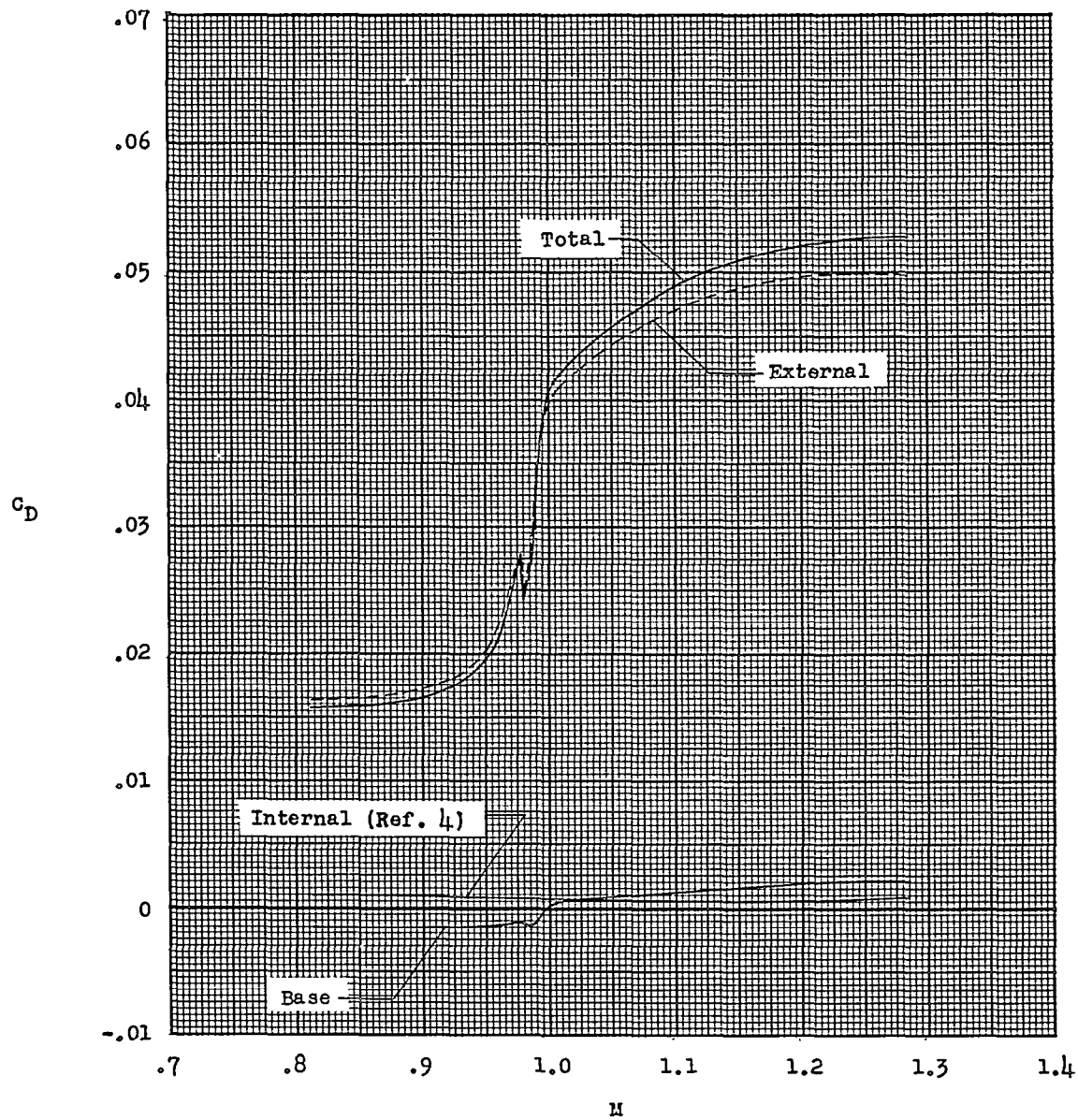

Figure 9.- Summary of drag data for rocket model 3 varying with Mach number (based on wing included area).